Deformation and Fracture of Urethane–Methacrylate Resins

R. H. ELLEITHY,[1] A. HILTNER,[1,*] E. BAER,[1] I. M. FRASER,[2] and M. L. ORTON[2]

[1]Department of Macromolecular Science and Center for Applied Polymer Research, Case Western Reserve University, Cleveland, OH 44106; [2]ICI Acrylics, Wilton Middlesbrough, Cleveland TS6 8JE, England

SYNOPSIS

The tensile properties of three urethane–methacrylate resins that varied in the soft segment content of the urethane were characterized. The strain birefringence at a circular hole was observed during loading–unloading cycles to progressively higher displacements. The shear strain distribution at the hole was calculated from the isochromatic fringe contours and compared with results from linear elastic analysis. When the onset of nonlinearity, and the subsequent appearance of residual strain at the root of the hole, were correlated with features of the macroscopic stress-displacement curves, three regions of prefracture deformation were defined. A region of linear elastic behavior was observed at the lowest strains. The maximum shear strain at the linear limit was the same in all the resins, and appeared to correlate with the yield condition at the hole. When the shear strain at the hole exceeded about 2.8%, the fringe patterns started to deviate from the elastic prediction. However, strain was fully recoverable in this region as indicated by the absence of residual birefringence at the hole after unloading. This region of nonlinear, recoverable deformation extended to progressively higher strains as the amount of urethane soft segment increased. This feature was attributed to the network structure of the urethane–methacrylate resins. A region characterized by nonrecoverable deformation at the hole followed at higher strains; the urethane soft segment content had a major effect on the amount of permanent deformation sustained before fracture. The fracture surfaces exhibited features typical of brittle fracture without crazing. © 1995 John Wiley & Sons, Inc.

INTRODUCTION

Uniaxial tests can be misleading when the purpose is to characterize prefracture deformation of relatively brittle materials in tension. When fracture is controlled by flaws, the tendency for premature catastrophic failure can preempt irreversible deformation mechanisms intrinsic to the material. The blunt notch is particularly attractive when the objective is to localize deformation while minimizing the tendency for crack growth. The moderate stress intensification and gradual stress gradient at the root of a blunt notch minimize the tendency for premature brittle fracture. The circular notch geometry is particularly attractive for studying prefracture damage since an exact numerical solution of the elastic stress field distribution over a fairly large region around the notch is available. Finally, the circular notch geometry can be machined accurately while causing minimal predamage.

A few examples illustrate how the circular notch has found broad applicability in the study of prefracture deformation of polymers. When the material is optically transparent, an analysis of the strain birefringence at a circular notch provides a quantitative description of linear and nonlinear behavior.[1] At higher strains, analysis of the damage zone that forms at a circular notch during slow tensile loading can reveal the conditions for craze initiation and growth,[2,3] clarify the shear yielding modes in ductile polymers,[4] or, in polymer blends, elucidate the factors that control competition between shear yielding and cavitation mechanisms.[5]

The goal of this study was to characterize the deformation of some urethane-methacrylate resins. After curing, these resins consist of a crosslinked network that contains both urethane and methyl methacrylate segments.[6,7] In the series of resins

* To whom correspondence should be addressed.

Journal of Applied Polymer Science, Vol. 55, 1395–1404 (1995)
 CCC 0021-8995/95/101395-10

studied, the amount of soft segment in the urethane component was varied. The resulting resins exhibited a significant range in stiffness and ductility. Because they were optically transparent, it was possible to characterize their tensile properties by observing the strain birefringence at a circular hole during loading–unloading cycles to progressively higher strains.

MATERIALS AND METHODS

The urethane–methacrylate resins were provided by ICI Acrylics in the form of sheets 3 and 4 mm thick. Methyl methacrylate was copolymerized with methacrylate end-capped urethane in a ratio of 1-to-1 by weight. The soft segment content of the urethane was varied from 0% to 13% to 21% w/w. The resulting three resins are identified as S0, S13 and S21, respectively. The urethane methacrylates were polyfunctional, and copolymerized with methyl methacrylate to form a three-dimensional network. Poly(methyl methacrylate) (PMMA) was Acrylite FF from CYRO Industries, Mt. Arlington, NJ, and the thermoplastic polyurethane was Isoplast 302 from Dow Chemical USA, Midland, MI.

Dynamic mechanical properties were measured with the DMTA Mark II from Polymer Laboratories (Amherst, MA) operating in the tensile mode at a frequency of 1Hz. Measurements were made over the temperature range −150° to 200°C with a heating rate of 3°C/min. The specimens were 3.5 mm thick, 4–5 mm wide, and 40 mm long. The quantities tan δ and E' are reported.

Type I, dogbone tensile specimens were milled from the 3-mm-thick sheets. Edges and surfaces of the specimens were polished first with increasingly fine grades of sandpaper and then with aqueous suspensions of alumina powder, the finest being 1 micron, to a final width of 12.5 mm and final thickness of 2.5 mm. The specimens were then conditioned at 100°C for 30 h. A 1-mm-radius circular hole was drilled in the center of the gauge section of some of the tensile specimens before they were polished and conditioned.

The tensile behavior of specimens with and without a hole was determined by loading to fracture in an Instron mechanical testing machine at a strain rate of 0.1%/min. Strain was measured with a 2.5 cm mechanical extensometer. Three specimens of each composition were tested. Fracture surfaces were examined in the optical microscope.

To determine the strain optical coefficient, unnotched tensile specimens were positioned between the polarizer and analyzer of a polariscope and stretched at a rate of 0.1%/min to a maximum of 0.5% strain. The progressive color changes were noted and each color was assigned a stress level according to[8,9]

$$c = \frac{\delta}{t\sigma} \tag{1}$$

where c is the stress optical coefficient, δ is the relative retardation,[8] t is the thickness, and σ is the applied stress. The measurements were carried out in triplicate. The strain optical coefficient k was then calculated from

$$k = \frac{cE}{(1 + \upsilon)} \tag{2}$$

where E is Young's modulus. The Poisson's ratio of PMMA, $\upsilon = 0.35$, was used.

To determine the shear strain distribution at a circular hole, the specimen was positioned between the polarizer and analyzer of the polariscope and repeatedly loaded and unloaded to a gradually increasing displacement at a rate of 0.1%/min. The displacement was typically increased by about 0.2 mm on each successive cycle. The fringe pattern at the hole was photographed at the maximum load and at the unloaded position of each cycle. Because the extensometer could not be used with these experiments, the displacement was taken from the position of the crosshead. The experiment was repeated with nine specimens of each composition and the results of a typical experiment are reported.

The shear strain distribution at the maximum load was calculated from the fringe pattern

$$\varepsilon_{xy}\,(\%) = \frac{\delta\,100}{kt} \tag{3}$$

The shear strain along the x-axis calculated from eq. (3) was compared with that from elasticity theory[10,11]

$$\varepsilon_{xy}\,(\%) = \frac{(1 + \upsilon)(\sigma_1 - \sigma_2)100}{E} \tag{4}$$

where σ_1 and σ_2 are the principal stresses.

Compact tension specimens were milled from the 4-mm-thick plates. The specimens were 49 mm wide and 41 mm long in accordance with ASTM E399; a sharp edge crack about 21 mm in length was induced with a sharp razor blade using a very slow cutting

speed, 1 mm/h. Three specimens of each composition were loaded in tension to fracture with a crosshead speed of 100 mm/min so the fracture occurred within 60 s of loading. The critical stress intensity factor K_{Ic} was calculated according to[12]

$$K_{Ic} = \sigma\sqrt{\mathbf{a}}F \tag{5}$$

where **a** is the crack length and F is a geometric factor. The critical energy release rate G_{Ic} was then calculated as

$$G_{Ic} = \frac{(K_{Ic})^2}{E} \tag{6}$$

where E is Young's modulus.

RESULTS AND DISCUSSION

Dynamic Mechanical and Stress–Strain Behavior

The temperature dependence of tan δ and E' is plotted in Figure 1. The large peak in tan δ, accompanied by a drop in E' of more than two orders of magnitude, identified the glass transition of the resins. The glass transition of S0 at 131°C was approximately 25° higher than the glass transition of PMMA due to constraint of the methyl methacrylate chains by the urethane crosslinks. The glass transition temperature decreased, approaching that of PMMA, as the amount of soft segment in the urethane increased. It follows that as the length of soft segment in the urethane crosslinks increased, the crosslinks provided less constraint to the methyl methacrylate

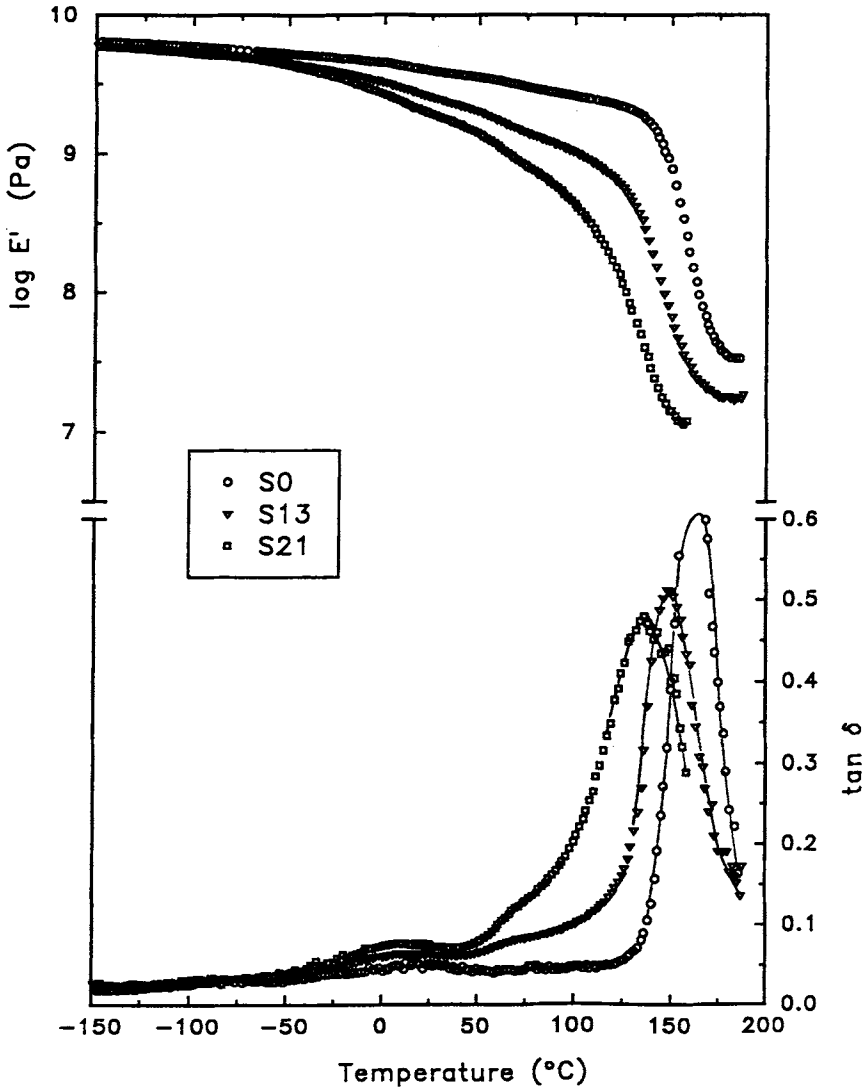

Figure 1 Dynamic mechanical behavior of urethane–methacrylate resins.

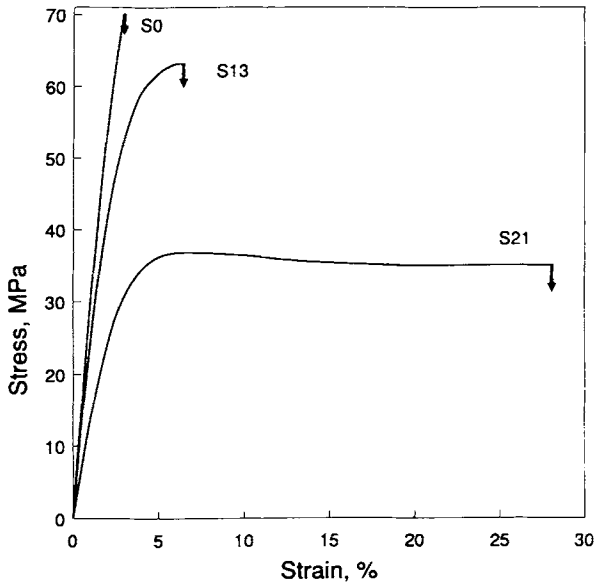

Figure 2 Stress–strain curves of urethane–methacrylate resins.

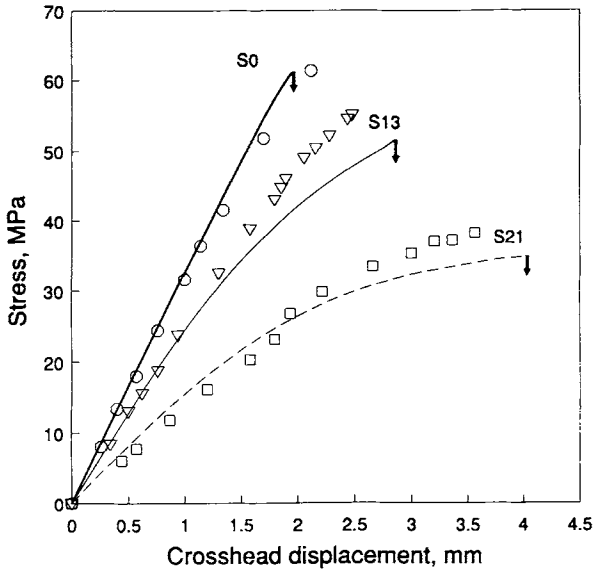

Figure 3 Stress-displacement relationship of urethane–methacrylate resins with a center hole. The curves refer to single loading experiments; the individual points mark the maximum stress and corresponding displacement of successive loading–unloading cycles.

chains and their flexibility approached that of linear PMMA chains. The tan δ peak also broadened as it shifted to lower temperatures in S0, S13 and S21, and in addition a shoulder developed at about 70°C. The relationship between the intensity of the shoulder and the composition of the urethane indicated that it was associated with the urethane soft segment.

Stress–strain curves for the three urethane–methacrylate polymers are compared in Figure 2. The initial linear region of the stress–strain curve reflected the decrease in modulus with increasing urethane soft segment content. The values decreased from 3.6 to 2.5 to 1.7 GPa for S0, S13, and S21, respectively (Table I). For comparison, moduli of PMMA and a thermoplastic polyurethane are included in Table I. The modulus of S0 was close to that of PMMA; the somewhat lower moduli of S13 and S21 were in the same range as the thermoplastic polyurethane. At approximately 1% strain the stress–strain curve became nonlinear with a gradually decreasing modulus. Shortly after the onset of nonlinear behavior, composition S0 fractured in a brittle manner. The fracture strain was about 3%. The nonlinear region of S13 extended to a higher strain with fracture at about 6% strain. The fracture stress of S13 was slightly lower than that of S0. The stress–strain curve of S21 exhibited a broad maximum, followed by a region of constant stress that extended to fracture at 28% strain. Extension was uniform through the gauge section with no indication of necking or other localized deformation. Most of the strain was recovered after fracture. The moduli measured for these three materials were in the range reported for other urethane–methacrylate

Table I Properties of Urethane Methacrylate Resins

Resin	Modulus (GPa)	Yield Stress (MPa)	Fracture Stress (MPa)	Fracture Strain (%)	T_g (°C)	Strain Optical Coefficient
S0 (MODAR 805)	3.6 ± 0.3	93	70	2.9	131	0.059–0.072
S13 (MODAR 835)	2.5 ± 0.2	56	63	6.3	118	0.040–0.053
S21 (MODAR 835(21)HE)	1.7 ± 0.1	34	36	28.0	110	0.023–0.030
PMMA (Acrylite FF)	3.1 ± 0.2	—	—	—	—	0.010–0.011
PU (Isoplast 302)	2.2 ± 0.1	—	—	—	—	0.065–0.078

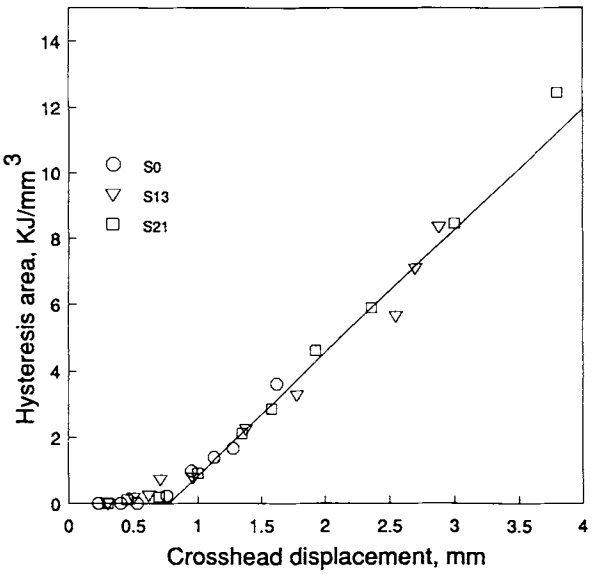

Figure 4 Hysteresis on successive loading–unloading cycles as a function of maximum displacement.

resins, typically 2.2–4.6 GPa.[13] Fracture strains were higher, however: 3% for the most brittle resin S0 compared to 0.7–1.6% quoted in the previous study. This might suggest that a urethane–methacrylate prepolymer of higher functionality was used in the study cited. It was also true that the brittle resins including S0 were very sensitive to surface flaws, so extreme care was required in the preparation of tensile specimens.

Stress-displacement curves of Type I specimens with a circular hole monotonically loaded to fracture are compared in Figure 3. In general, the trends with composition were the same as with unnotched tensile bars. The initial slope and the fracture stress decreased with increasing urethane soft segment; conversely, the non-linearity and extension at fracture increased. Specimens with a circular hole were also cyclically loaded to progressively higher displacement, and the results are included in Figure 3 as data points marking the maximum stress and corresponding displacement for each cycle. Although the displacement was determined from the position of the machine crosshead, the data points lay close to the monotonic loading curves where the displacement was taken from an extensometer. The coincidence was especially good at lower stresses. At higher stresses, when hysteresis and nonrecoverable extension in the loading–unloading cycle indicated plastic deformation at the hole, especially for compositions S13 and S21, the data points lay above the monotonic loading curve.

The hysteresis area for each cycle is plotted in Figure 4. Linear elastic behavior with no hysteresis was observed in the first few cycles. After the initial cycles, the hysteresis area increased linearly with displacement. Data for all three compositions are superimposed on a single line; a least-squares fit in the range between 1 and 3 mm identifies the linear limit at 0.77 mm displacement. The relationship between hysteresis loss and strain was virtually the same for the three resins; the difference was the displacement and hysteresis area on the last cycle before fracture, which increased with the amount of urethane soft segment.

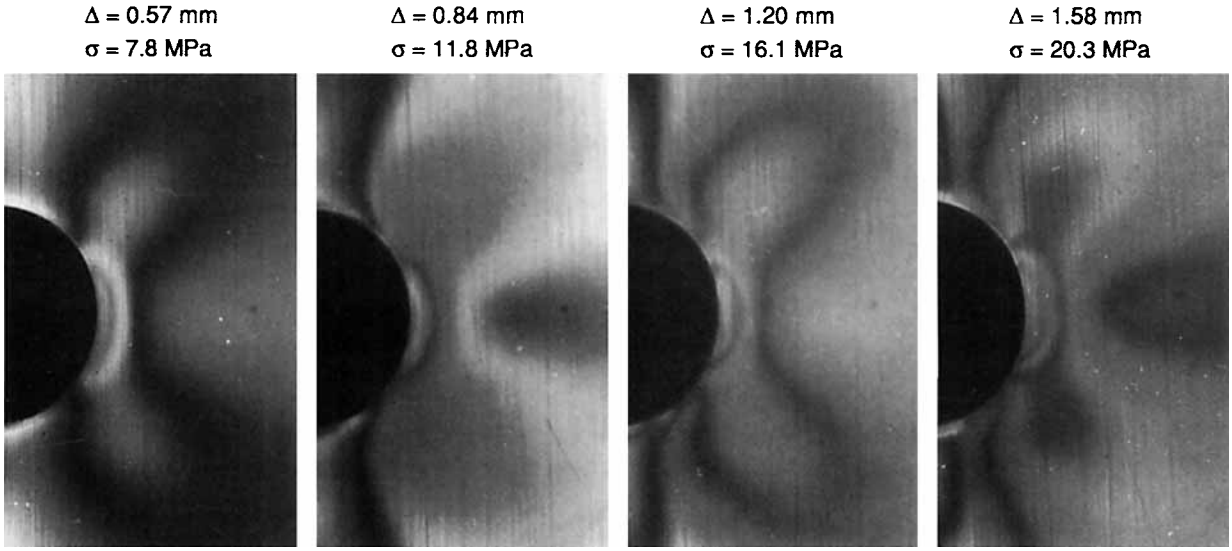

Figure 5 Strain birefringence patterns at a center hole in composition S21.

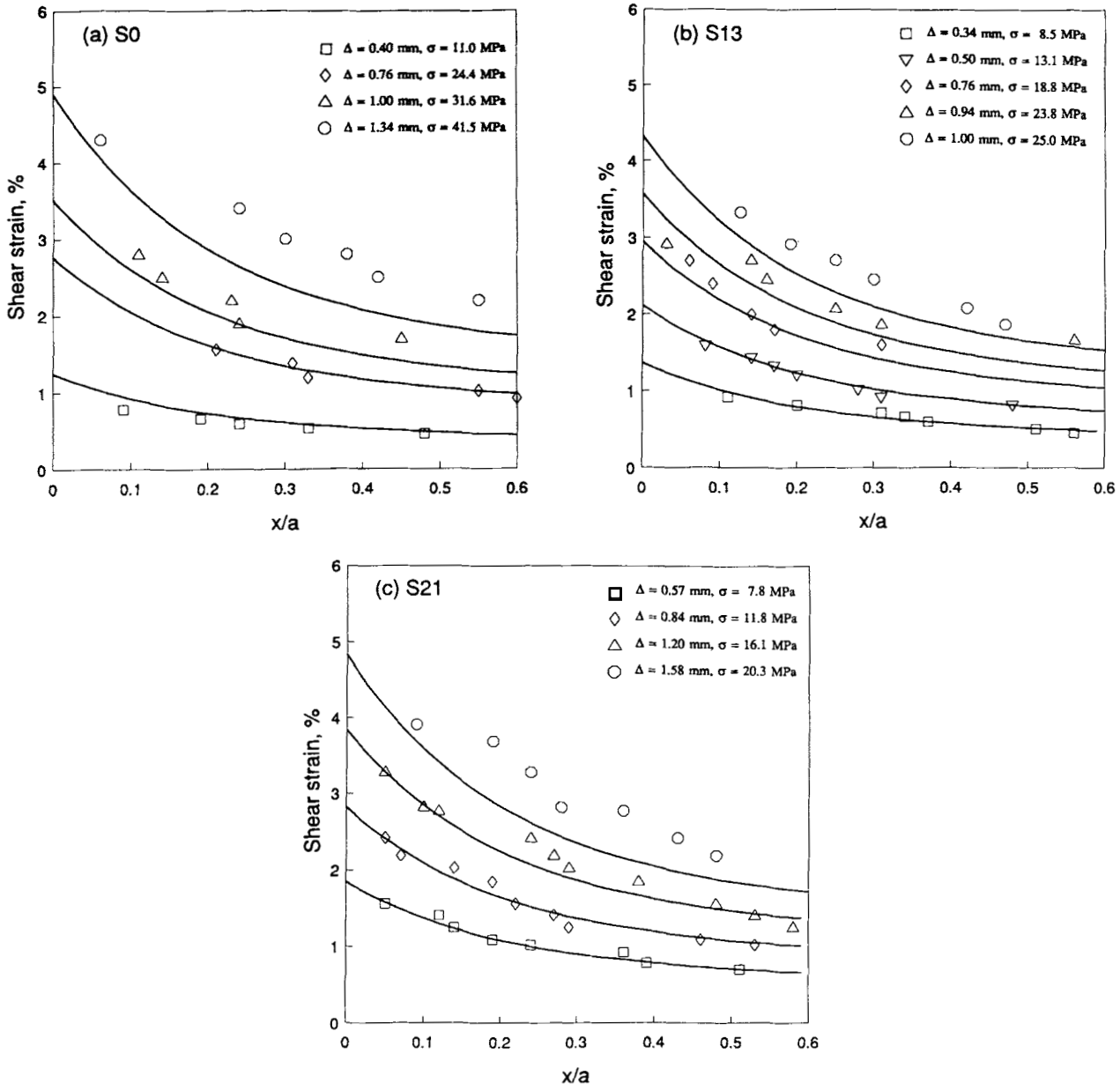

Figure 6 Shear strain distribution along the x-axis, determined from the fringe patterns (points) compared with the calculated elastic shear strain (solid curves): (a) S0, (b) S13, and (c) S21. The remote stress (σ) and the crosshead displacement (Δ) are indicated.

Strain Birefringence

Typical examples of the strain birefringence at the hole are shown in Figure 5. The photographs were taken at the maximum stress on consecutive loading–unloading cycles of S21. The strain optical coefficient (k), needed to calculate the shear strain distribution along the x-axis from the fringes, was measured directly by straining unnotched tensile bars. The values obtained for the urethane–methacrylate resins were intermediate between those of PMMA linear homopolymer and a thermoplastic polyurethane (Table I). The decrease in the coefficient k from S0 to S21 indicated a decrease in photoelastic sensitivity; in other words, the identical fringe pattern corresponded to lower shear strains in S0 than in S21.

The shear strain along the x-axis at the maximum displacement in the loading–unloading cycle, calculated from eq. (3), is compared with the elastic shear strain calculated from the infinite plate solution in Figure 6. The correlation was excellent for

the first few cycles. The loading–unloading curves on these cycles were also linear; recovery was complete and there was no hysteresis. Some deviation was apparent when the shear strain at the notch root exceeded 2.8%. The beginning of nonlinearity was indicated when strains calculated from the fringe patterns fell above the elastic curve. The strain distribution from the fringe pattern showed a characteristic "hump" at $x/\mathbf{a} = 0.4$ which coincided with the cubic point in the elastic stress distribution.

In other materials, specifically polycarbonate and a thermoplastic polyurethane, deviation of the measured shear strain from the elastic solution was first observed when the yield stress was achieved at the hole. The remote stress required for yielding at the hole was estimated from the tensile yield stress and the von Mises yield criterion with the octahedral shear stress concentration factor at a circular hole of 1.26 in plane strain. Using values of the tensile yield stress from Table I, the remote stress required to achieve the yield condition at the hole was calculated to be 35.4 MPa, 21.3 MPa, and 12.9 MPa for S0, S13, and S21, respectively. For the latter two compositions, these values were very close to the remote stress at the linear limit as determined from the fringe analysis. The value of 35.4 MPa calculated for S0 was significantly larger than 24 MPa, the remote stress when the linear limit was reached at the hole in this composition. The quoted value was estimated from the plane strain compressive yield strength and possibly was in error. With the assumption that the elastic limit corresponded to the yield condition at the hole, a value of 75 MPa was obtained for the tensile yield stress of S0.

Only two regions of deformation were considered in the previous study of PC and a thermoplastic polyurethane: an initial linear elastic region where the strain at the hole was described by elastic theory, followed by plastic deformation after the yield condition was reached at the hole. The region of yielding was identified from the residual birefringence at the hole. Nonrecoverable deformation was also detected in the urethane–methacrylate resins beginning as a small area of residual birefringence that remained at the hole after the specimen was unloaded. However, the urethane–methacrylate resins had to be cycled to stresses and strains considerably higher than the linear limit before residual strain was observed at the hole. The remote stress on the loading–unloading cycle when residual birefringence was first observed was 52 MPa, 45 MPa, and 33 MPa for S0, S13, and S21, compared to 24 MPa, 19 MPa, and 12 MPa, respectively, at the linear limit. It appears that there is an intermediate region where deformation of the urethane–methacrylate resins is nonlinear but recoverable.

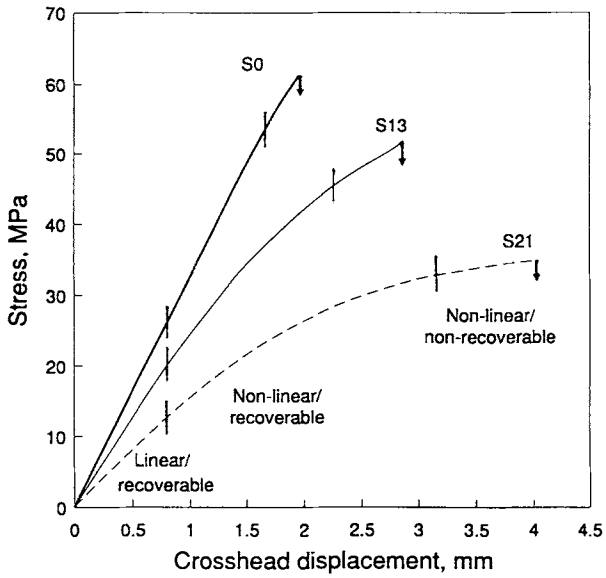

Figure 7 Stress-displacement curves with the three regions of deformation indicated.

The three regions are indicated on the stress-displacement curves in Figure 7. The initial elastic region is characterized by a linear stress-displacement relationship, no hysteresis in the cyclic loading–unloading curve, and complete recoverability of the strain. The linear limit is the same for the three urethane–methacrylate resins, and occurs at a crosshead displacement of 0.77% which corresponds to a maximum shear strain of 2.8% at the hole. From comparisons with similar experiments in the literature, the linear limit of the urethane–methacrylate resins is determined to be about the same as for other engineering plastics. The linear elastic region is followed by a region of nonlinear, recoverable deformation. The lower boundary of this region is defined by deviation of the shear strain distribution from elastic theory, and the upper boundary by the appearance of residual strain at the hole. In between, the relationship between stress and strain is not linear, but no residual birefringence is detected when the stress is removed. This transitional region may also occur in polycarbonate and the thermoplastic polyurethane. It is, however, more conspicuous in the urethane–methacrylate resins where it extends to progressively higher strains as the amount of soft segment in the urethane increases. The capacity to recover from high strains is attributed to the network structure of the urethane–methacrylate resins. Especially if the urethane crosslinks contain a flexible soft segment, they accommodate extension of the

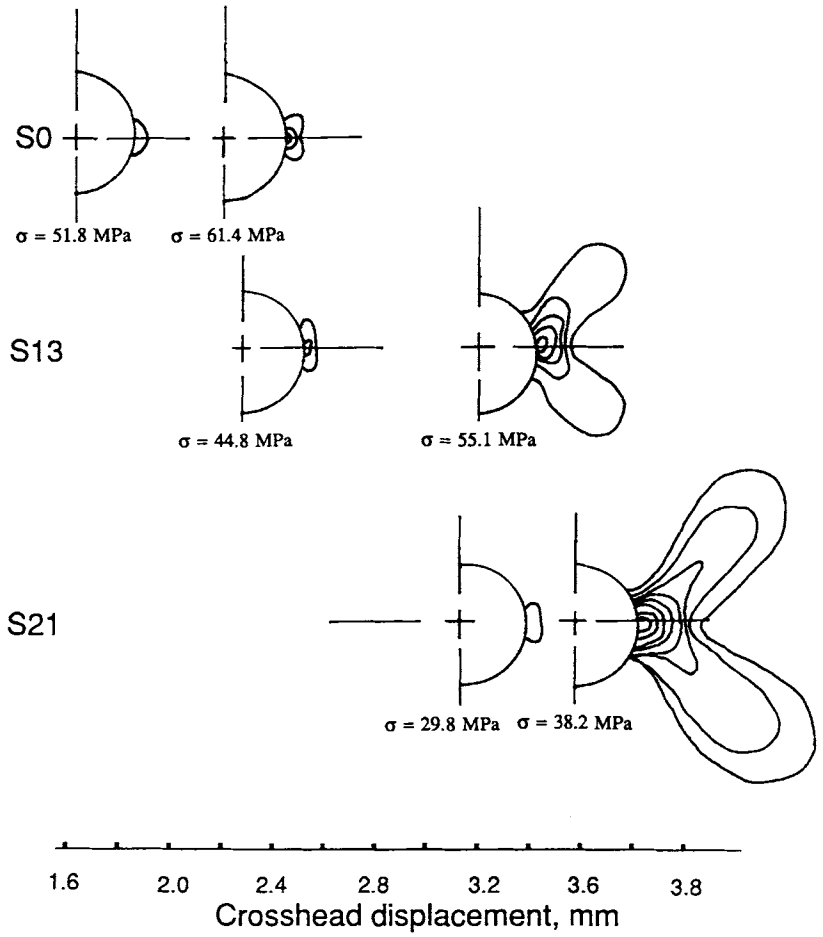

Figure 8 Sketches of the residual strain birefringence patterns at a center hole. The crosshead displacement is indicated on the abscissa.

methyl methacrylate chains and then enhance the strain recovery.

The contours of the residual birefringence patterns are compared in Figure 8. Only a small area of birefringence developed at the hole before the S0 composition fractured. The amount of permanent deformation sustained before fracture increased with the soft segment content of the urethane. The residual strain pattern of S21 closely resembled that of the thermoplastic polyurethane where the strain was broadly distributed, rather than that of polycarbonate where the residual strain was concentrated at the hole.[1] These differences reflected the true stress–true strain behavior of the materials. The gradually expanding plastic zone of the urethane–methacrylate resins was characteristic of an elastic–plastic material with work-hardening, in contrast to a material that exhibits a yield instability with plastic flow.

Fracture

The urethane–methacrylate resins exhibited characteristics typical of brittle fracture. Tensile specimens of S0 always fractured with a bifurcated crack path which is a feature of very brittle fracture. Composition S13 sometimes fractured with bifurcation, in comparison to S21 which always fractured with a single crack plane perpendicular to the loading direction. The crack initiated at one side of the hole; the fracture surfaces of cyclically loaded specimens that contain the crack initiation site are shown in Figure 9.

It is not unusual for a fracture surface to show a sequence of different fracture markings, especially a tensile fracture surface where stress intensification and crack speed continually increase as the crack propagates. Crack initiation and propagation left distinct features on the fracture surfaces of the ure-

thane–methacrylates that were used to locate the fracture origin and deduce the progression of crack growth. Fracture of S21 in Figure 9(a) initiated at the lower edge of the hole, where a flaw created a stress concentration. The roughly semicircular region surrounding the initiation site is relatively smooth, thus this region is termed the "mirror" region. The initial flaw grew subcritically until the stress state reached a critical condition. Radial striations growing out from the origin indicate that growth proceeded along several cracks on slightly different planes. A short distance into the mirror region, a line demarcates the transition from subcritical flaw growth to catastrophic crack propagation. Initially, the slowly propagating crack front traveled radially and the surface formed was concave and approximately semicircular. The length of this region approximately coincided with the dimension of the prefracture plastic zone as defined by the residual birefringence on the cycle immediately preceeding fracture.

As the fracture accelerated beyond the semicircular region, the propagating crack interacted with the microstructure and the stress field to produce a region of increasing roughness. The parabolic markings that characterize this region point back toward the initiation site. They were created by interaction of the primary crack with secondary cracks that initiated at flaws in response to the high stress concentration created by the primary crack. A dense array of interacting and overlapping secondary cracks produced the progressively more complex patterns as the crack speed increased.

The smaller mirror region and rougher fracture surface of S13 in Figure 9(b) indicate that this composition was more brittle than S21. The roughness was produced by numerous overlapping secondary cracks that point back toward the initiation site. The fracture of S0 in Figure 9(c) was even more brittle. The mirror region is too small to be seen at this magnification and a complex pattern of secondary crack initiation begins almost at the initiation site. Further from the initiation site, the texture created by multiple crack initiation becomes so dense that directionality relative to the initiation site is lost.

None of the fracture surfaces exhibited the craze features that are characteristic of PMMA.[14] The features that characterized the fracture surfaces of the urethane–methacrylate resins are usually indicative of fracture that is more brittle than crazing fracture. The conventional fracture toughness parameters for the urethane–methacrylate resins in Table II were consistent with brittle fracture and comparable to the reported fracture toughness of PMMA (K_{Ic} = 1.2).[15] Furthermore, the parameters K_{Ic} and G_{Ic} indicated that composition S0 was more brittle than S13 or S21.

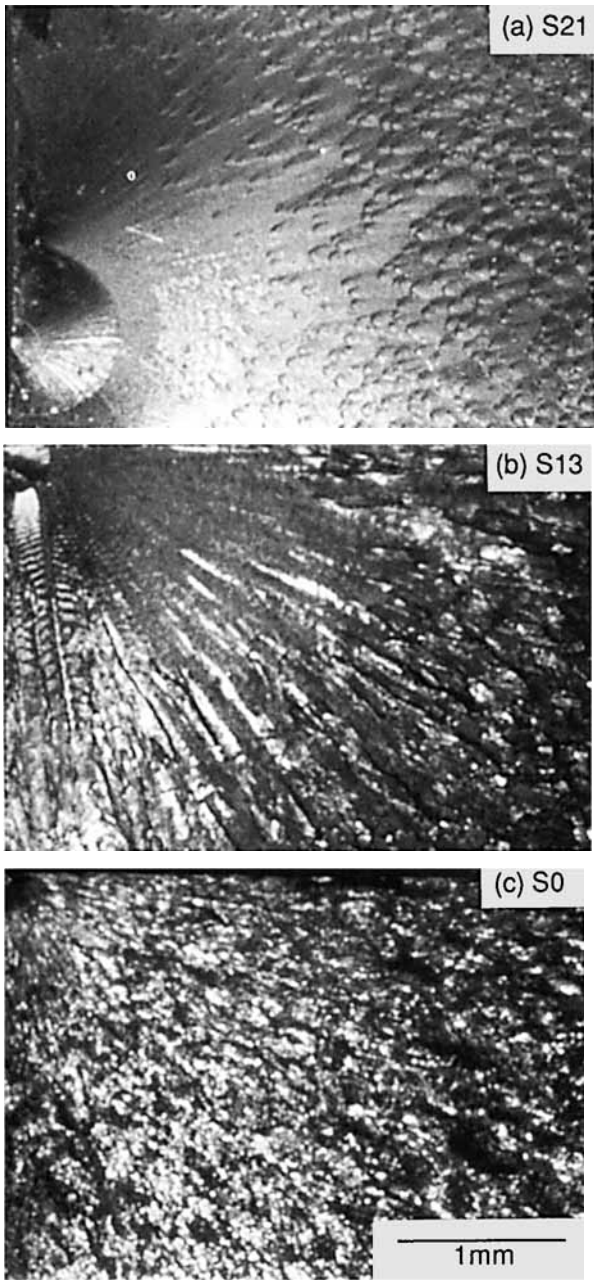

Figure 9 Optical micrographs showing the fracture surfaces of urethane-methacrylate resins with a center hole cyclically loaded to fracture: (a) S21, (b) S13, and (c) S21. The half that contains the initiation site is shown with the edge of the hole to the left.

Table II Crack Propagation Resistance of Urethane Methacrylate Resins

Resin	Modulus (MPa)	Critical Stress Intensity Factor K_{Ic} (MPa $m^{1/2}$)	Critical Energy Release Rate G_{Ic} (J m^2)
S0	3.6 ± 0.3	0.69 ± 0.21	132
S13	2.5 ± 0.2	1.33 ± 0.24	708
S21	1.7 ± 0.1	1.13 ± 0.21	751

CONCLUSIONS

The tensile properties of three urethane–methacrylate resins that varied in the amount of soft segment in the urethane were characterized by examining the deformation at a circular hole during slow tensile loading. This approach was particularly useful for observing nonlinear and yielding behavior of resins that tended to be brittle in tension. Based on an analysis of the strain birefringence that accompanied cyclic loading, three regions of prefracture deformation were defined:

1. A region of linear elastic behavior was observed at the lowest strains. The stress distribution calculated from the isochromatic fringe contours satisfactorily fit a linear elastic analysis. The stress-displacement relationship was linear in this region and there was no measurable hysteresis in the loading–unloading curves. The maximum shear strain at the linear limit was the same for all the resins, and appeared to correlate with the yield condition at the hole. The coincidence of nonlinearity with the yield condition was observed previously for polycarbonate and a thermoplastic polyurethane, and may be a general result.
2. A transitional region followed the linear elastic limit. When the shear strain at the hole exceeded about 2.8%, the fringe patterns began to deviate from the elastic curve. This coincided with nonlinearity in the stress-displacement relationship and measurable hysteresis in the loading–unloading curve. However, strain was fully recoverable in this region as indicated by the absence of residual birefringence at the hole after unloading. This region of nonlinear, recoverable deformation was more prominent in the urethane–methacrylate resins than in polycarbonate or a thermoplastic polyurethane. It extended to progressively higher strains as the amount of soft segment in the urethane increased. Strain recovery in this region was an attribute of the network structure of the urethane–methacrylate resins.
3. A region characterized by nonrecoverable deformation at the hole followed the non-linear, recoverable region. The gradually expanding plastic zone was typical of an elastic–plastic material with work-hardening. The amount of permanent deformation sustained before fracture increased with the soft segment content of the urethane. The resulting fracture surfaces exhibited features typical of brittle fracture without crazing.

This research was generously supported by ICI Chemicals & Polymers Limited through the Edison Polymer Innovation Corp. (EPIC).

REFERENCES

1. C. Kau, A. Tse, A. Hiltner, and E. Baer, *J. Mater. Sci.*, **28,** 529 (1993).
2. M. Ishikawa, H. Ogawa, and I. Narisawa, *J. Macromol. Sci.-Phys.*, **B19,** 421 (1981).
3. E. S. Shin, A. Hiltner, and E. Baer, *J. Appl. Polym. Sci.*, **46,** 213 (1992).
4. M. Ma, K. Vijayan, J. Im, A. Hiltner, and E. Baer, *J. Mater. Sci.*, **24,** 2687 (1989).
5. C. Cheng, A. Hiltner, E. Baer, P. R. Soskey, and S. G. Mylonakis, *J. Appl. Polym. Sci.*, **52,** 177 (1994).
6. C. B. Bucknall, X. C. Zhang, M. L. Orton, and G. V. Jackson, *J. Appl. Polym. Sci.*, **52,** 457 (1994).
7. M. L. Orton, I. M. Fraser, and S. H. Rogers, *Eng. Plastics*, **2,** 274 (1989).
8. M. M. Frocht, *Photoelasticity*, Vol. I, Wiley, New York, 1941.
9. R. B. Heywood, *Designing by Photoelasticity*, Chapman & Hall, London, 1952.
10. J. W. Dally and W. F. Rilley, *Experimental Stress Analysis*, 3rd ed., McGraw-Hill, New York, 1991.
11. S. Timoshenko and J. N. Goodier, *Theory of Elasticity*, 3rd ed., McGraw-Hill, New York, 1968.
12. H. Tada, *The Stress Analysis of Cracks Handbook*, 2nd ed., Paris Productions, St. Louis, 1985.
13. T. Sterrett, R. Wong, and P. Kidd, *Polym. Eng. Sci.*, **27,** 669 (1987).
14. W. Doell, in *Fractography and Failure Mechanisms of Polymers and Composites*, Chap. 10, A. C. Roulin-Moloney, Ed., Elsevier, London, 1989.
15. W.-M. Cheng, G. A. Miller, J. A. Manson, R. W. Hertzberg, and L. H. Sperling, *J. Mater. Sci.*, **25,** 1917 (1990).

Received July 7, 1994
Accepted August 2, 1994